CHEMISTRY OF MATERIALS

25th Anniversary

Article

Functional Polymer Brushes on Hydrogenated Graphene

Max Seifert, Amelie H. R. Koch, Frank Deubel, Tobias Simmet, Lucas H. Hess,
Martin Stutzmann, Rainer Jordan, Jose Antonio Garrido, and Ian D. Sharp

Just Accepted

ACS Publications

High quality. High impact.

Functional Polymer Brushes on Hydrogenated Graphene

Max Seifert[#], Amelie H. R. Koch[#$], Frank Deubel[$], Tobias Simmet[#], Lucas H. Hess[#], Martin Stutzmann[#], Rainer Jordan[$°], José A. Garrido[#] and Ian D. Sharp[#*%]

Walter Schottky Institut and Physik Department, Technische Universität München, Am Coulombwall 4, 85748 Garching, Germany

$ Wacker-Lehrstuhl für Makromolekulare Chemie, Technische Universität München, Lichtenbergstrasse 4, 85748 Garching, Germany

° Professur für Makromolekulare Chemie, Department Chemie, Technische Universität Dresden, Zellescher Weg 19, 01069 Dresden, Germany

% Current address: Joint Center for Artificial Photosynthesis, Lawrence Berkeley National Laboratory, 1 Cyclotron Rd., Berkeley, CA 94720

ABSTRACT: We demonstrate that the degree of hydrogenation of graphene directly controls the grafting density and thus, the layer thickness of grafted polymer brushes synthesized via self-initiated photografting and photopolymerization. Among the tested monomers, only styrene derivatives could be directly grafted onto copper-supported graphene. Therefore, copolymerization of styrene and acrylates, as well as consecutive grafting of both monomer types, was employed to realize functional polymer brushes of poly(styrene-co-acrylate) copolymers. The direct grafting of polymers on graphene results in polymer carpets that are suitable for a wide variety of applications.

Introduction

The extraordinary mechanical, optical, thermal, and electrical properties of graphene[1] make this two-dimensional (2D) material a unique candidate for a broad variety of applications.[2,3] In particular, given its exceptional chemical and mechanical stability, as well as unique electrical properties such as low noise and high ambipolar charge carrier mobility,[4] graphene is an extremely promising platform for biosensors.[5,6] So far, these properties have been exploited for fabrication of devices capable of monitoring pH changes,[7] protein adsorption,[8] action potentials of cells[9] and glucose sensing.[10] In order to use graphene in biological environments, as well as to improve sensing specificity and device sensitivity, a well-defined functionalization method for graphene is required. Since the unique properties of graphene arise from sp^2 hybridization of carbon in a 2D geometry, non-covalent modifications based on π-π stacking or ionic interactions have been developed in order to realize good dispersion and accessibility to the graphene sheet.[11–14] However, for long term and reliable use of graphene-based devices in demanding biological environments a robust, irreversible modification is required. Therefore, multiple strategies for covalent modification of graphene have been successfully developed,[15] including the hydrogenation to gra-

phane,[16–19] the fluorination to fluorographene,[20,21] the oxidation to graphene oxide,[22,23] and the spontaneous grafting of diazonium salts,[24–28] which are facile methods for introducing chemical functions for further modification. However, as the functionalization results in conversion of sp^2 to sp^3-carbon, direct attachment of chemical moieties to the 2D-graphene framework must be balanced with the desired modulation of the electronic properties of graphene. Moreover, the large reactivity differences for covalent addition onto the basal plane versus the edges of graphene make a defined modification difficult.

Recently, we demonstrated that graphene can be directly modified by covalent grafting of polymer brushes using self-initiated photografting and photopolymerization (SIPGP).[29] It was found that this facile *grafting from* polymerization, using only UV-light, bulk monomer, and graphene, results in homogeneous polymer brushes on the basal plane of single, few, and multiple layer graphene. The resulting composite is referred to as a polymer carpet, comprised of a single graphene sheet as the substrate and a densely grafted polymer brush. Scanning confocal Raman spectroscopy showed that grafting occurs only from residual defect sites. Furthermore, we found that the photografting process is selective for aromatic monomers (styrene), while acrylates do not result in detectable

1

polymer layer formation. In order to further develop this method, additional control of the brush layer morphology, as well as introduction of other vinyl monomers, is necessary. In this account, we show that the poly(styrene) brush layer thickness can be directly controlled by the degree of hydrogenation of the graphene used for SIPGP. Moreover, we show the grafting of different styrene derivatives on pristine graphene to demonstrate the general feasibility of this process for a range of monomers. Finally, two alternative routes to polymer brushes comprised of styrene and acrylate monomer units are presented. Both aspects are crucial steps towards the development of functional graphene-based materials for biosensing.

Experimental Section

CVD graphene growth and transfer: Graphene films were grown by chemical vapor deposition on copper foil.[30,31] The copper foil was pre-annealed at 1000°C under a flow of 28 sccm hydrogen for 20 min. Thereafter, graphene was grown for 30 min under a flow of 3.5 sccm methane and 16 sccm hydrogen at a total pressure of 10 mbar. Then, the copper-graphene foil was cooled to room temperature under growth atmosphere. For transfer of non-photopolymerized material, samples were spin-coated with poly(methylmethacrylate) (PMMA) and floated on 0.5 M aqueous $FeCl_3$ solution overnight to selectively remove the copper foil. Afterwards, the films were rinsed with deionized water and transferred to a 300 nm thick SiO_2 layer on silicon. PMMA was removed by thorough rinsing in acetone and isopropanol and dried with a jet of nitrogen. For the transfer of functionalized samples the as-grown polymer carpet was sufficient as supportive layer and no additional spin-coated PMMA layer was necessary.

Graphene hydrogenation: Hydrogenation of the as-grown graphene films was achieved in a remote DC hydrogen plasma system at 0.1 mbar of H_2 flow. Samples were placed 15 cm from the plasma discharge region, facing away from the plasma to prevent physical damage by energetic ions. A variable acceleration voltage, V_{acc}, was applied between the sample holder and the plasma electrodes. All samples were hydrogenated for 20 min. Graphene films for Raman spectroscopy characterization were hydrogenated after transfer to SiO_2. Graphene films used for polymerization experiments were hydrogenated while still on the Cu foil to avoid contamination from PMMA before polymerization.

Surface photopolymerization: Polymerization was performed following a procedure introduced by Steenackers et al.[29] Graphene on Cu foil was submerged in ~0.5 mL of distilled and degassed bulk monomer (monomer mixture in the case of copolymerization) and irradiated with an UV fluorescent lamp with a spectral distribution between 300 and 400 nm ($\lambda(I_{max})$ = 350 nm with a total power of ~5 mW/cm^2). Following SIPGP, the functionalized films were thoroughly rinsed with different solvents (e.g. toluene, ethyl acetate, and ethanol for the case of pure styrene) in order to remove all physisorbed polymer.

Raman spectroscopy: Raman spectra were recorded using the 514.5 nm line of an Ar ion laser in a micro-Raman spectroscopy setup with approx. 3 mW/μm^2 at the sample. Spectra were integrated for 300 s for each spectral window. Linear background subtraction of residual fluorescence was performed when necessary.

Fourier transform infrared spectroscopy: Infrared spectroscopy was performed following polymerization of CVD-grown graphene using an IFS Bruker Vertex 70 instrument, equipped with a diffuse reflectance infrared Fourier transform (DRIFT) setup from SpectraTech and a liquid nitrogen-cooled MCT detector. For each spectrum, 100 scans were accumulated with a spectral resolution of 4 cm^{-1}. The measurements were performed on functionalized CVD graphene after transfer onto 300 nm SiO_2 on Si. For each measurement, background spectra were recorded on bare 300 nm SiO_2 on Si

Atomic force microscopy (AFM): AFM scans were performed with a multimode scanning probe microscope from Veeco Instruments, using standard tips in tapping mode under ambient conditions. The polymer brush layers were scratched with a sharp tip and the surfaces were scanned over 5 x 5 μm^2 to determine the step height at the scratch edge.

Results and Disussion

The effect of hydrogenation on the graphene film quality was investigated by Raman spectroscopy. Figure 1A shows Raman spectra of a graphene sheet before hydrogenation (black), after hydrogenation at V_{acc} =-260 V (red), and after annealing at 450°C for 24 h (blue). The G band at 1580 cm^{-1} and the 2D band at 2680 cm^{-1} are characteristic features of pristine graphene, corresponding to the in-plane vibrational mode and the two-phonon intervalley double resonance scattering, respectively.[32,33] A single Lorentzian shape of the 2D peak and a G/2D Raman mode intensity ratio of <1 suggest the predominant presence of single layer graphene. The D band near 1340 cm^{-1} is attributed to a defect-activated intervalley double resonance. Its relative intensity can be used as a measure of the density of defects in graphene. After hydrogenation, the intensity of the D band drastically increases compared to the G band. Furthermore the D' mode, which is correlated to a defect-activated intravalley double resonance process, arises near 1620 cm^{-1}. These changes can be attributed to the partial conversion of lattice sites from the C-C sp^2- to the C-H sp^3-binding configuration. After annealing, the spectrum almost completely recovers to its initial state, which is consistent with the expectations for graphane formation[16] and confirms that hydrogen incorporation is the origin of enhanced defect density. In agreement with previous work, the spectrum of the post-annealed sample shows an increase of the defect-related mode intensity relative to the as-grown case of approx. 50%, which may originate from residual bound hydrogen on the graphene sheet.[19,18] Figure 1B illustrates the evolution of the D/G Raman mode intensity ratio after hydrogenation as a function of the remote plasma acceleration voltage. The intensity ratio I_D/I_G and, in turn, the amount of surface-bound hydrogen, continuously increases with increasingly negative values of V_{acc}. At V_{acc} = -300 V, I_D/I_G reaches a value of ~3.7. According to Cancado et al.,[34] such a value corresponds to an average distance of ~3 nm between neighboring hydrogenated sites and, thus to a coverage of <1% of a monolayer. Control measurements (green data points) on graphene, hydrogenated while still on the Cu foil, confirm that hydrogenation of graphene on Cu foil occurs in a similar way to hydrogenation of graphene on SiO_2.
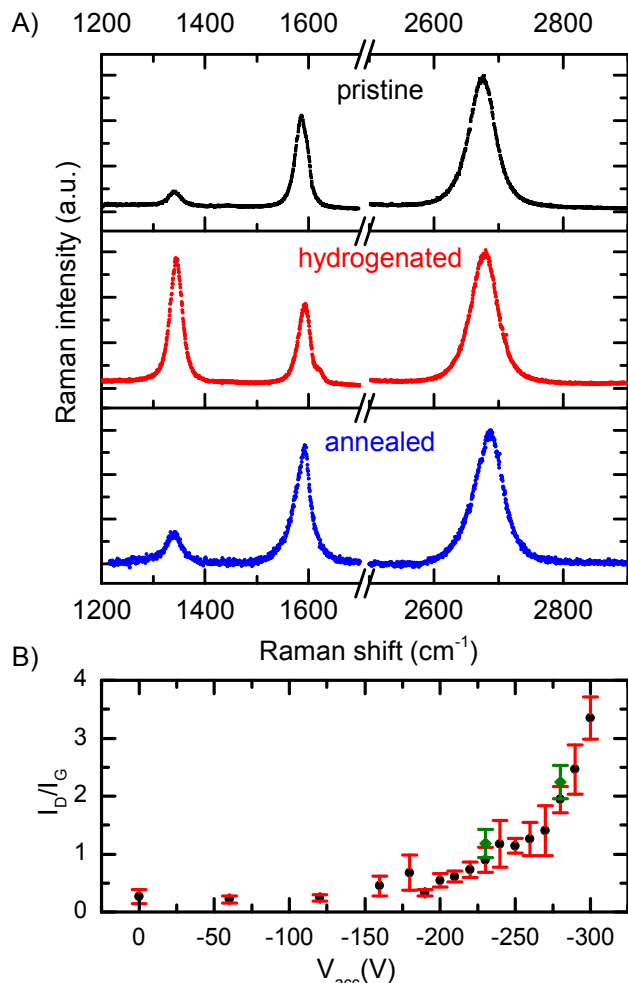
2

Figure 1 (A) Raman spectra of a graphene film transferred onto a 300 nm thick SiO_2 layer on Si. Spectra were recorded before hydrogenation (black), after hydrogenation at V_{acc} =-260 V (red), and after annealing at 450°C for 24 h (blue). (B) D/G Raman mode intensity ratio as a function of remote plasma acceleration voltage for graphene hydrogenated on SiO_2 (black) and Cu foil (green). Data from three measurement locations per sample were averaged for each point and the standard deviations were used to obtain the error bars.

Recently, the SIPGP has been used successfully for the preparation of polymer brushes on various material such as polymers[35–37] or self-assembled monolayers,[38] without the need of a dedicated surface-bound initiator system. In fact, very early reports already described the photografting onto various kinds of substrates.[39–42] The SIPGP relies on abstractable groups preferably with low bond-dissociation energy and is, as such, ideal for the direct functionalization of carbonaceous material such as glassy carbon,[43] e-beam generated carbon deposits (carbon templating),[44] silicon carbide[45] or diamond.[46] In contrast, pristine graphene is composed of pure sp^2-hybridized carbon and should exhibit no photoreactivity for SIPGP. However, we previously demonstrated that photografting initiates from residual sp^3-carbon defect sites on the graphene basal-plane, though it was not possible to establish the specific identity of those sites at that time.[29] In the present work, a systematic variation of the sp^3-defect density by hydrogenation provides a means to directly control the polymer brush grafting

density. Based on this concept, we have applied the photopolymerization process to pristine graphene and hydrogenated graphene with different hydrogen site coverage obtained by variation of the acceleration voltage in the plasma reactor, as shown in Figure 1B. Figure 2A shows DRIFT spectra of a polystyrene (PS) layer, polymerized on pristine graphene for t = 16 h. Characteristic vibrational modes of PS are observed, including the aromatic groups (v_{C-H} at ~3025 cm^{-1} and $v_{C=C}$ between 1450 cm^{-1} and 1602 cm^{-1}). The characteristic modes of the methylene groups of the polystyrene backbone appear at v_{C-H} ~2921 cm^{-1}.[47] The discontinuous structure of the resulting PS layer can be seen in in the scanning electron micrograph in Figure 2B.
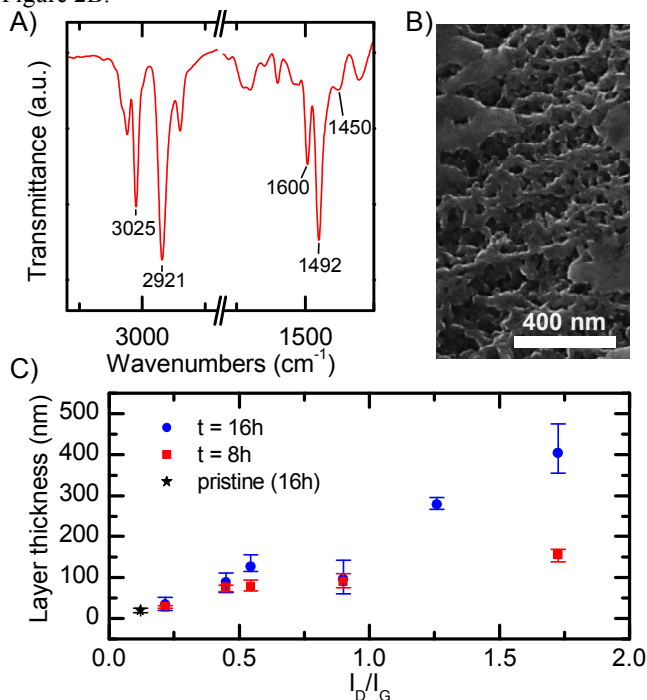

Figure 2 (A) Diffuse reflectance IR (DRIFT) spectra of styrene polymerized for 16 h on pristine graphene showing characteristic vibrational modes of the aromatic groups, v_{C-H} at ~3025 cm^{-1} and $v_{C=C}$ between 1450 cm^{-1} and 1602 cm^{-1}, as well as the methylene C-H stretching modes of the polymer backbone at 2921 cm^{-1}. (B) Scanning electron microscopy image of PS network grown on pristine graphene on Cu. (C) Thickness of polystyrene layer as a function of the D/G Raman mode intensity ratio for polymerization times of 16 h (blue circles) and 8 h (red squares).

The PS layer thickness, as determined by AFM, versus the D/G Raman mode intensity ratio is plotted in Figure 2C for polymerization times of 16 h (blue circles) and 8 h (red squares). The layer thickness for pristine graphene (black star) after 16 h of polymerization is shown for comparison. For both polymerization times, the layer thickness on hydrogenated material increases with increasing I_D/I_G ratio. According to the scaling law for terminally grafted polymer layers,[48] the polymer layer thickness increases with increasing grafting density because of surface crowding. Considering Figure 1B and Figure 2C, the large aerial density of hydrogen sites on the surface, corresponding to a high I_D/I_G ratio, correlates well with the observed systematic increase of the polymer layer thickness. This suggests that C-H sp^3-sites on graphene act as primary initiation points for polymer chain growth and

3

demonstrates that the grafting density and layer thickness can be directly controlled by the degree of hydrogenation of graphene over a wide range, with collapsed brush thicknesses from a few nm up to approximately 400 nm. In terms of the electronic properties of the functionalized graphene, we have previously shown that, as no additional defects are induced upon polymer grafting, the polymerization reaction itself only affects the level of doping but does not significantly degrade the carrier mobilities.[29] Hydrogenation, however, introduces C-H sp[3]-sites and is thus known to negatively affect the electronic transport properties.[49]

In previous work, we observed that out of a range of different vinyl monomers, including MMA and 4-vinylpyridine, only styrene resulted in noticeable grafting on graphene. Again, we find a similar reactivity contrast on hydrogenated graphene; while reaction of styrene proceeds in a highly controllable and reproducible fashion, no reaction of methacrylates is observed. In addition, we performed SIPGP with other styrene derivatives such as 4-bromostyrene and pentafluorostyrene and observed considerable grafting for both monomers on as-grown graphene and hydrogenated graphene. We obtained growth rates of ~6.7 nm/h for pentafluorostyrene and ~30 nm/h for 4-bromostyrene on pristine graphene, compared to ~2.1 nm/h for styrene. Layer growth rates are reproducible and the SIPGP of both monomers resulted in the first examples of poly(pentafluorostyrene) and poly(4-bromostyrene) layer directly grafted on graphene and hydrogenated graphene. While the first provides a chemical handle for further functionalization, the second polymer carpet is an alternative approach to the fluorination of graphene. At this point, we do not know the chemical or physical reason for the selective reactivity of styrenics with graphene or hydrogenated graphene. As the polarity of styrene, pentafluorostyrene and 4-bromostyrene is very different, a wetting phenomenon might not play a dominant role. Furthermore, since 4-vinylpyridine is not reactive, π-π stacking is an unlikely origin. Currently, we are further investigating this intriguing aspect of the SIPGP process on graphene and hydrogenated graphene. In order to overcome this limitation of SIPGP-graftable monomers on graphene, we used copolymerization of styrene with acrylic monomers. Although MMA cannot initiate polymerization on bare or hydrogenated graphene, MMA is expected to grow from other organic material, given the presence of abstractable hydrogen atoms and/or already growing chains. Considering the copolymerization reactivity ratios for styrene and MMA (both r~0.5), a statistical copolymer is expected to form in the presence of both monomers. Figure 3A outlines the copolymerization grafting process starting with styrene. SIPGP copolymer grafting was performed in a mixture of bulk styrene (S) and MMA for 24 h, both on pristine graphene, as well as hydrogenated graphene. The presence of MMA monomer units in the resulting copolymer layer could be unambiguously confirmed by DRIFT spectroscopy. Figure 3B shows the typical DRIFT spectra of a P(S-co-MMA) brush (black) and of pure styrene (red), both polymerized on hydrogenated graphene for 24 h. The characteristic vibrational modes of PS are observed in both spectra, whereas for the copolymer (black), the methylene groups of MMA dominate the spectrum between 2946 cm^{-1} and 2988 cm^{-1}.[38] In addition, the strong carbonyl stretch at 1731 cm^{-1} clearly confirms the presence of MMA units and thus the formation of a copolymer layer.
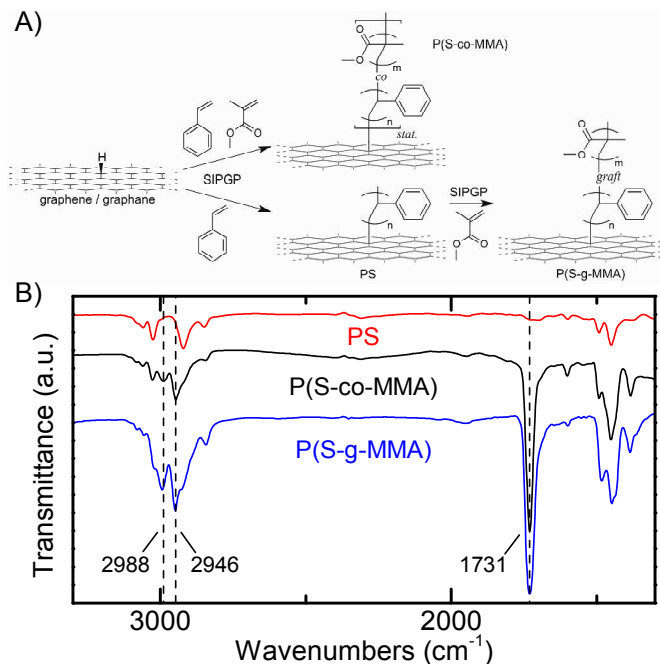

Figure 3 (A) Schematic illustration of the copolymerization process via SIPGP. (B) DRIFT spectra of a pure PS brush (red), a P(S-co-MMA) copolymer layer (black) and a P(S-g-MMA) graft-copolymer layer (blue) on hydrogenated graphene. Dashed lines indicate the additional vibrational bands originating from MMA monomer units.

The obtained growth rate of the P(S-co-MMA) copolymer on pristine graphene of ~1.9 nm/h corresponds well to the value of ~2.1 nm/h observed for the styrene homografting, indicating that the initiation is the rate limiting reaction step. As PS is not miscible with PMMA, further modification, such as saponification of the acrylate might be difficult. Hence, we additionally performed a two-step SIPGP grafting starting with styrene grafting on graphene (16 h) to give a PS carpet with a thickness of approx. 30 nm and a consecutive SIPGP with bulk MMA for 5 h onto the PS carpets. While the copolymerization of both monomers resulted in a total carpet thickness of < 50 nm after 24 h irradiation with UV, the two-step grafting resulted in a ~135 nm thick P(S-g-MMA) copolymer layer after 16+5 h. The presence of PMMA was again verified by DRIFT (blue curve in Figure 3B). Because of the faster polymerization rate of MMA, the consecutive SIPGP using a thin PS primer layer is preferable if a thicker and more accessible PMMA is desired.

Conclusion

In conclusion, remote hydrogen plasma treatment was applied to finely tune the concentration of surface-bound hydrogen and, in turn, polymer brush grafting density. Using this approach, it is possible to achieve a well-controlled balance between the density of functional groups on the surface and defect sites in the graphene. Furthermore, these results are in accordance with the earlier hypothesized grafting mechanism of styrene on graphene by SIPGP. Moreover, we have demonstrated statistical- as well as graft-copolymerization of styrene and MMA on graphene and hydrogenated graphene, thus opening a crucial synthetic route to functional polymer brushes on graphene. In principle, this approach can be further

4

expanded to all monomers that are polymerizable by SIPGP,[38] thus enabling the preparation of stimuli-responsive polymer carpets[50,51] based on graphene.

ASSOCIATED CONTENT

AUTHOR INFORMATION

Corresponding Author

*E-Mail: idsharp@lbl.gov

REFERENCES

(1)   Novoselov, K. S.; Geim, A. K.; Morozov, S. V.; Jiang, D.; Zhang, Y.; Dubonos, S. V.; Grigorieva, I. V.; Frisov, A. A. *Science*. **2004,** *306* (5696), 666–669.

(2)   Geim, A. K.; Novoselov, K. S. *Nat Mater*. **2007,** *6* (3), 183–191.

(3)   Singh, V.; Joung, D.; Zhai, L.; Das, S.; Khondaker, S. I.; Seal, S. *Progress in Materials Science*. **2011,** *56* (8), 1178–1271.

(4)   Hess, L. H.; Hauf, M. V.; Seifert, M.; Speck, F.; Seyller, T.; Stutzmann, M.; Sharp, I. D.; Garrido, J. A. *Appl. Phys. Lett.* **2011,** *99* (3), 33503.

(5)   Kuila, T.; Bose, S.; Khanra, P.; Mishra, A. K.; Kim, N. H.; Lee, J. H. *Biosensors and Bioelectronics*. **2011,** *26* (12), 4637–4648.

(6)   Dankerl, M.; Hauf, M. V.; Lippert, A.; Hess, L. H.; Birner, S.; Sharp, I. D.; Mahmood, A.; Mallet, P.; Veuillen, J.-Y.; Stutzmann, M.; Garrido, J. A. *Adv. Funct. Mater.* **2010,** *20* (18), 3117–3124.

(7)   Ang, P. K.; Chen, W.; Wee, A. T. S.; Loh, K. P. *J. Am. Chem. Soc.* **2008,** *130* (44), 14392–14393.

(8)   Ohno, Y.; Maehashi, K.; Yamashiro, Y.; Matsumoto, K. *Nano Lett*. **2009,** *9* (9), 3318–3322.

(9)   Hess, L. H.; Jansen, M.; Maybeck, V.; Hauf, M. V.; Seifert, M.; Stutzmann, M.; Sharp, I. D.; Offenhäusser, A.; Garrido, J. A. *Adv. Mater*. **2011,** *23* (43), 4968.

(10) Kwak, Y. H.; Choi, D. S.; Kim, Y. N.; Kim, H.; Yoon, D. H.; Ahn, S.-S.; Yang, J.-W.; Yang, W. S.; Seo, S. *Biosensors and Bioelectronics*. **2012,** *37* (1), 82–87.

(11) Su, Q.; Pang, S.; Alijani, V.; Li, C.; Feng, X.; Müllen, K. *Adv. Mater*. **2009,** *21* (31), 3191–3195.

(12) Liang, Y.; Wu, D.; Feng, X.; Müllen, K. *Adv. Mater*. **2009,** *21* (17), 1679–1683.

(13) Choi, E.-Y.; Han, T. H.; Hong, J.; Kim, J. E.; Lee, S. H.; Kim, H. W.; Kim, S. O. *J. Mater. Chem*. **2010,** *20* (10), 1907.

(14) Das, S.; Irin, F.; Tanvir Ahmed, H.; Cortinas, A. B.; Wajid, A. S.; Parviz, D.; Jankowski, A. F.; Kato, M.; Green, M. J. *Polymer*. **2012,** *53* (12), 2485–2494.

(15) Yan, L.; Zheng, Y. B.; Zhao, F.; Li, S.; Gao, X.; Xu, B.; Weiss, P. S.; Zhao, Y. *Chem. Soc. Rev*. **2011,** *41* (1), 97.

(16) Castellanos-Gomez, A.; Wojtaszek, M.; Arramel; Tombros, N.; van Wees, B. J. *Small*. **2012,** *8* (10), 1607–1613.

(17) Sun, Z.; Pint, C. L.; Marcano, D. C.; Zhang, C.; Yao, J.; Ruan, G.; Yan, Z.; Zhu, Y.; Hauge, R. H.; Tour, J. M. *Nat Comms*. **2011,** *2*, 559.

(18) Elias, D. C.; Nair, R. R.; Mohiuddin, T. M. G.; Morozov, S. V.; Blake, P.; Halsall, M. P.; Ferrari, A. C.; Boukhvalov, D. W.; Katsnelson, M. I.; Geim, A. K.; Novoselov, K. S. *Science*. **2009,** *323* (5914), 610–613.

(19) Ryu, S.; Han, M. Y.; Maultzsch, J.; Heinz, T. F.; Kim, P.; Steigerwald, M. L.; Brus, L. E. *Nano Lett*. **2008,** *8* (12), 4597–4602.

(20) Robinson, J. T.; Burgess, J. S.; Junkermeier, C. E.; Badescu, S. C.; Reinecke, T. L.; Perkins, F. K.; Zalalutdniov, M. K.; Baldwin, J. W.; Culbertson, J. C.; Sheehan, P. E.; Snow, E. S. *Nano Lett*. **2010,** *10* (8), 3001–3005.
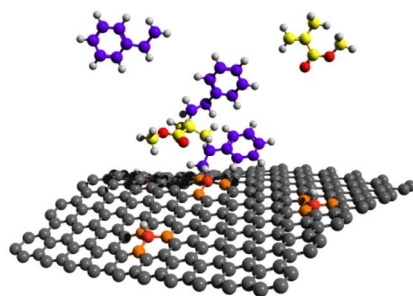
(21) Lee, W. H.; Suk, J. W.; Chou, H.; Lee, J.; Hao, Y.; Wu, Y.; Piner, R.; Akinwande, D.; Kim, K. S.; Ruoff, R. S. *Nano Lett*. **2012,** *12* (5), 2374–2378.

(22) Hummers, W. S.; Offeman, R. E. *J. Am. Chem. Soc*. **1958,** *80* (6), 1339.

(23) Cote, L. J.; Cruz-Silva, R.; Huang, J. *J. Am. Chem. Soc.* **2009,** *131* (31), 11027–11032.

(24) Anariba, F.; DuVall, S. H.; McCreery, R. L. *Anal. Chem.* **2003,** *75* (15), 3837–3844.

(25) Lomeda, J. R.; Doyle, C. D.; Kosynkin, D. V.; Hwang, W.-F.; Tour, J. M. *J. Am. Chem. Soc.* **2008,** *130* (48), 16201–16206.

(26) Bekyarova, E.; Itkis, M. E.; Ramesh, P.; Berger, C.; Sprinkle, M.; Heer, W. A. de; Haddon, R. C. *J. Am. Chem. Soc.* **2009,** *131* (4), 1336–1337.

(27) Sharma, R.; Baik, J. H.; Perera, C. J.; Strano, M. S. *Nano Lett.* **2010,** *10* (2), 398–405.

(28) Lim, H.; Lee, J. S.; Shin, H.-J.; Shin, H. S.; Choi, H. C. *Langmuir.* **2010,** *26* (14), 12278–12284.

(29) Steenackers, M.; Gigler, A. M.; Zhang, N.; Deubel, F.; Seifert, M.; Hess, L. H.; Lim, C. H. Y. X.; Loh, K. P.; Garrido, J. A.; Jordan, R.; Stutzmann, M.; Sharp, I. D. *J. Am. Chem. Soc.* **2011,** *133* (27), 10490–10498.

(30) Li, X.; Cai, W.; An, J.; Kim, S.; Nah, J.; Yang, D.; Piner, R.; Velamakanni, A.; Jung, I.; Tutuc, E.; Banerjee, S. K.; Colombo, L.; Ruoff, R. S. *Science.* **2009,** *324* (5932), 1312–1314.

(31) Liu, W.; Li, H.; Xu, C.; Khatami, Y.; Banerjee, K. *Carbon.* **2011,** *49* (13), 4122–4130.

(32) Malard, L.; Pimenta, M.; Dresselhaus, G.; Dresselhaus, M. *Physics Reports.* **2009,** *473* (5-6), 51–87.

(33) Ferrari, A. C. *Solid State Communications.* **2007,** *143* (1-2), 47–57.

(34) Cançado, L. G.; Jorio, A.; Ferreira, E. H. M.; Stavale, F.; Achete, C. A.; Capaz, R. B.; Moutinho, M. V. O.; Lombardo, A.; Kulmala, T. S.; Ferrari, A. C. *Nano Lett.* **2011,** *11* (8), 3190–3196.

(35) Deng, J.-P.; Yang, W.-T.; Rånby, B. *Macromolecular Rapid Communications.* **2001,** *22* (7), 535-538.

(36) Wang, H.; Brown, H. R. *Macromol. Rapid Commun.* **2004,** *25* (11), 1095–1099.

(37) Stachowiak, T. B.; Svec, F.; Fréchet, J. M. J. *Chem. Mater.* **2006,** *18* (25), 5950–5957.

(38) Steenackers, M.; Küller, A.; Stoycheva, S.; Grunze, M.; Jordan, R. *Langmuir.* **2009,** *25* (4), 2225–2231.

(39) Taylor, H. S.; Vernon, A. A. *J. Am. Chem. Soc.* **1931,** *53* (7), 2527–2536.

(40) Wright, A. N. *Nature.* **1967,** *215* (5104), 953–955.

(41) White, P. *Proc. Chem. Soc.* **1961** (September), 337–338.

(42) Braun, D.; Kamprath, A. *Angew. Makromol. Chemie.* **1984,** *120* (1), 1–41.

(43) Zhang, N.; Steenackers, M.; Luxenhofer, R.; Jordan, R. *Macromolecules.* **2009,** *42* (14), 5345–5351.

(44) Steenackers, M.; Jordan, R.; Küller, A.; Grunze, M. *Adv. Mater.* **2009,** *21* (28), 2921–2925.

(45) Steenackers, M.; Sharp, I. D.; Larsson, K.; Hutter, N. A.; Stutzmann, M.; Jordan, R. *Chem. Mater.* **2010,** *22* (1), 272–278.

(46) Steenackers, M.; Lud, S. Q.; Niedermeier, M.; Bruno, P.; Gruen, D. M.; Feulner, P.; Stutzmann, M.; Garrido, J. A.; Jordan, R. *J. Am. Chem. Soc.* **2007,** *129* (50), 15655–15661.

(47) Jordan, R.; Ulman, A.; Kang, J. F.; Rafailovich, M. H.; Sokolov, J. *J. Am. Chem. Soc.* **1999,** *121* (5), 1016–1022.

(48) Milner, S. T. *Science.* **1991,** *251* (4996), 905–914.

(49) Burgess, J. S.; Matis, B. R.; Robinson, J. T.; Bulat, F. A.; Keith Perkins, F.; Houston, B. H.; Baldwin, J. W. *Carbon.* **2011,** *49* (13), 4420–4426.

(50) Amin, I.; Steenackers, M.; Zhang, N.; Schubel, R.; Beyer, A.; Gölzhäuser, A.; Jordan, R. *Small.* **2011,** *7* (5), 683–687.

(51) Amin, I.; Steenackers, M.; Zhang, N.; Beyer, A.; Zhang, X.; Pirzer, T.; Hugel, T.; Jordan, R.; Gölzhäuser, A. *Small.* **2010,** *6* (15), 1623–1630.

6

Insert Table of Contents artwork here

A)

B)

A)

B)